AD-A209 836

REPORT DOCUMENTATION PAGE

Form Approved OMB No. 0704-0188

(2)

DTIC ELECTE JUL 1 0 1989 S D H

Field	Entry
1a. REPORT SECURITY CLASSIFICATION	UNCLASSIFIED
1b. RESTRICTIVE MARKINGS	
2a. SECURITY CLASSIFICATION AUTHORITY	
2b. DECLASSIFICATION / DOWNGRADING SCHEDULE	
3. DISTRIBUTION / AVAILABILITY OF REPORT	Approved for public release; distribution unlimited.
4. PERFORMING ORGANIZATION REPORT NUMBER(S)	
5. MONITORING ORGANIZATION REPORT NUMBER(S)	AFOSR-TR- 89-0934
6a. NAME OF PERFORMING ORGANIZATION	Princeton University
6b. OFFICE SYMBOL (If applicable)	
7a. NAME OF MONITORING ORGANIZATION	AFOSR/NE
6c. ADDRESS (City, State, and ZIP Code)	Department of Electrical Engineering, Princeton University, Princeton, NJ 08544
7b. ADDRESS (City, State, and ZIP Code)	Bldg. 410, Bolling Air Force Base, DC 20332
8a. NAME OF FUNDING / SPONSORING ORGANIZATION	AFOSR
8b. OFFICE SYMBOL (If applicable)	NE
9. PROCUREMENT INSTRUMENT IDENTIFICATION NUMBER	AFOSR-85-0204
8c. ADDRESS (City, State, and ZIP Code)	Building 410, Bolling AFB, DC 20332

10. SOURCE OF FUNDING NUMBERS

PROGRAM ELEMENT NO.	PROJECT NO.	TASK NO.	WORK UNIT ACCESSION NO.
61102F	2305	C1	

11. TITLE (Include Security Classification)
Transport and Submillimeter Wave Spectroscopy of $GaAs/Al_xGa_{1-x}$ and $In_xGa_{1-x}As$ Heterostructures

12. PERSONAL AUTHOR(S)
D.C. Tsui

13a. TYPE OF REPORT	13b. TIME COVERED	14. DATE OF REPORT (Year, Month, Day)	15. PAGE COUNT
Final	FROM 7/85 TO 9/88	June 16, 1989	41

16. SUPPLEMENTARY NOTATION

17. COSATI CODES			18. SUBJECT TERMS (Continue on reverse if necessary and identify by block number)
FIELD	GROUP	SUB-GROUP	

19. ABSTRACT (Continue on reverse if necessary and identify by block number)

This report summarizes the research carried out at Princeton University under Air Force Office of Scientific Research Contract No. 85-0204. The research emphasizes the physics of the electronic processes in $GaAs/Al_xGa_{1-x}As$ and $In_xGa_{1-x}As/InP$ heterojunction thin film structures and focuses in two directions: one in superlattice materials and the other in submillimeter wave spectroscopy. After a brief description is given of the accomplishments in both directions, together with a list of the publications of work supported by the contract, a detailed account is made of the systematic investigation of transport through $In_xGa_{1-x}As/InP$ superlattices grown by Chemical Beam Epitaxy.

20. DISTRIBUTION / AVAILABILITY OF ABSTRACT	21. ABSTRACT SECURITY CLASSIFICATION
☒ UNCLASSIFIED/UNLIMITED ☐ SAME AS RPT. ☐ DTIC USERS	UNCLASSIFIED

22a. NAME OF RESPONSIBLE INDIVIDUAL	22b. TELEPHONE (Include Area Code)	22c. OFFICE SYMBOL
Dr WITT	(202) 767-4931	NE

DD Form 1473, JUN 86 — Previous editions are obsolete. — SECURITY CLASSIFICATION OF THIS PAGE

89 7 10 065

AFOSR-TR- 89-0934

I. Introduction

This is a final report on the research carried out at Princeton University under the Air Force Office of Scientific Research Contract No. 85-0204. This research program, started in the summer of 1985, was designed to investigate systematically the interaction of submillimeter electromagnetic radiation with the charge carriers in semiconductor superlattices, built with $GaAs/Al_xGa_{1-x}As$ and $In_xGa_{1-x}As/InP$ heterojunction thin-film structures. The emphasis at the start was on the physics of the electronic processes in such quantum structures and our initial effort was focussed in two directions. One is in superlattice materials and the other in submillimeter wave spectroscopy, though the long range goal is the merging of the two when sufficiently high quality superlattices can be built for specific device applications, in our case, the application of such truly synthetic electronic materials for the generation and amplification of submillimeter waves. In Sec. II, the accomplishments in both directions are briefly summarized and a list is given of the publications of work supported by the contract. Sec. III is a more detailed description of our systematic investigation of transport through InGaAs-InP superlattices grown by Chemical Beam Epitaxy. These unpublished results are an up-to-date evaluation of the material quality of this superlattice system synthesized by using the most current materials technology.

II. Summary of Accomplishments

II.1. Superlattice materials

GaAs/$Al_xGa_{1-x}As$ has been the most widely used material system for heterojunction superlattice structures. However, $Al_xGa_{1-x}As$ is usually poor in crystalline quality and its optimum growth temperature is considerably different from that of GaAs. In the case of single interface and conventional multiple quantum well structures, where quantum confinement of electrons in the GaAs well is of prime interest, the material quality of the $Al_xGa_{1-x}As$ barriers is not essential. In our case, electron propagation through the barriers is essential to a truly electronic superlattice structure and the material quality of the barrier is just as important as that of the well. Consequently, we put a great deal of effort on characterizing and understanding the electrical properties of the alternative $In_{0.53}Ga_{0.47}As$/InP system, in which there is no obvious limit on the material quality of the InP barrier material. We started this effort in collaboration with Dr. W.T. Tsang of AT&T Bell Laboratories, who was to develop a new chemical beam epitaxy (CBE) system for $In_{0.53}Ga_{0.47}As$/InP, and have, through this collaboration, made the following accomplishments:

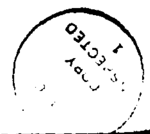

(a) High 2DEG mobility single quantum well structure of InGaAs/InP -- Confinement of a two-dimensional electron gas (2DEG) in a single quantum well (SQW) with two interfaces, though conceptually simple, has been a difficult experimental problem. In the case of the GaAs/$Al_xGa_{1-x}As$ heterostructure, the so-called "inverted HEMT" problem of the two interfaces causes strong asymmetry in confinement and serious deterioration of the 2DEG mobility. By utilizing the

Dist | Special
A-1

integer quantum Hall effect and the submillimeter wave cyclotron resonance as microscopic tools for the 2DEG and studying their changes with the different growth parameters, we have overcome such growth problems in the $In_{0.53}Ga_{0.47}As/InP$ system and achieved confinement of 2DEG in a SQW with mobility now in the range of $10^5 cm^2/Vsec$ (Publication 1).

(b) Double barrier resonant tunneling structures (DBRT) -- DBRTS, the simplest of heterostructures for exploring the basic physics in superlattices, have been widely studied using the $GaAs/Al_xGa_{1-x}As$ system and one long-standing problem is the asymmetry in I-V with respect to bias polarity. We have succeeded in the fabrication of DBRTS using InGaAs/InP and the observation of symmetric I-V. This is of considerable interest in that the structure can now be made on a 1.6μm wavelength optoelectronic material; but for us, it is an accomplishment indicating that the quality of the thin films, and especially the heterointerfaces, is sufficiently high for the manufacture and the investigation of the electronic properties of superlattices (Publication 2).

(c) High field transport in InGaAs/InP superlattices -- We have grown superlattices of $In_{0.53}Ga_{0.47}As/InP$ and studied their transport properties. The I-V characteristics beyond the initial ohmic regime show two series of sharp negative differential resistances (NDR's). They result from breakdown of the miniband conduction in the perpendicular direction in the presence of high electric fields and are a consequence of resonant tunneling between quantum levels in neighboring wells. The first series is due to tunneling from the ground to the first excited and the second series from the ground to the second excited levels in the neighboring

wells. The differential NDR's in each series are manifestations of an expanding high electric field domain through the entire sample. While the phenomenon is of fundamental importance to the understanding of electronic processes in a high electric field regime not encountered in bulk materials, more important to the goal of this research program is the indication that, in this high field limit, radiative decay may be a dominant channel for energy relaxation and that the structure may in fact be an efficient source for submillimeter wave radiation (Publication 4).

II.2. Submillimeter wave spectroscopy

Our effort on spectroscopy was, except for a short excursion to high T_c superconductors, focussed on the problem of magneto-absorption by the 2DEG in $GaAs/Al_xGa_{1-x}As$ single interface heterostructures. We have concentrated on the low density (n_s) and high mobility limit, where impurity effect is sufficiently reduced and electron-electron interactions are expected to be important, and made three contributions:

(a) We have observed cyclotron resonance (CR) in the extreme quantum limit when the Landau level filling factor $\nu \approx 0.08$ and studied ν dependence of the resonance line width (Γ). We found that the scattering time (τ_{CR}) deduced from Γ is ~10 times longer than that from dc transport and $\tau_{CR} \sim n_s^2$. Scattering is still dominated by impurities in GaAs and the observed n_s dependence of τ_{CR} must result from screening of the impurities by the 2DEG. Detailed account of this work is in publication 6.

(b) We also studied the T dependence of CR from 4.2 to 1.2K and observed a linear decrease of Γ with T together with a shift of the resonance towards a

lower magnet field.

(c) We have studied the effect of submillimeter wave on the magneto-transport of the 2DEG and identified their contributions to the observed photo-response: lattice heating, nonresonant electron heating, and electron heating by resonant absorption (Publication 8).

II.3. Publications of work supported by contract

1. Michel Frei, D.C. Tsui and W.T. Tsang, "Electronic properties of InGaAs/InP single quantum wells growth by chemical beam epitaxy," Appl. Phys. Lett. **50**, 609 (1987).

2. T.H.H. Vuong, D.C. Tsui and W.T. Tsang, "Tunneling in InGaAs-InP double-barrier structures," Appl. Phys. Lett. **50**, 212 (1987).

3. T.H.H. Vuong, D.C. Tsui and W.T. Tsang, "Dependence of the conduction in InGaAs/InP double-barrier tunneling structures on the mesa-etching process," Appl. Phys. Lett. **50**, 1004 (1987).

4. T.H.H. Vuong, D.C. Tsui and W.T. Tsang, "High field transport in an InGaAs/InP superlattice grown by chemical beam epitaxy," Appl. Phys. Lett. **52**, 981 (1988).

5. T.H.H. Vuong, D.C. Tsui and W.T. Tsang, "Resonant tunneling in InGaAs/InP double-barrier structures and superlattices," Superlattices and Microstructures **4**, 207 (1988).

6. M.J. Chou, D.C. Tsui and G. Weimann, "Cyclotron resonance high-mobility 2D electrons at extremely low densities," Phys. Rev. B **37**, 848 (1988).

7. M.J. Chou, D.C. Tsui and G. Weimann, "Cyclotron resonance in the extreme quantum limit," Surf. Sci. **196**, 279 (1988).

8. M.J. Chou, D.C. Tsui and A.Y. Cho, "FIR photoconductivity in the integral quantum Hall regime in GaAs/AlGaAs," Proc. 18th Intl. Conf. on Phys. of Semiconductors, 1986, ed. by O. Engstrom, p. 437.

9. T.H.H. Vuong, D.C. Tsui, V.J. Goldman, P.H. Hor, R.L. Meng, and C.W. Chu, "Far-infrared transmission spectra of high T_c superconductors," Solid State Commun. **63**, 525 (1987).

10. S. Prasad, H.P. Wei, D.C. Tsui, W. Schlapp and G. Weimann, "Transport and Persistent Photoconductivity in Atomic Planar Doped GaAs-AlAs/GaAs Heterostructures," J. Appl. Phys. **63**, 1793 (1988).

III. Transport Through InGaAs-InP Superlattices*

Recent advances in the growth of superlattices (SL's) have spurred many experimental studies on their transport properties, and on their application to novel devices. We have studied the perpendicular transport in superlattices of the InGaAs-InP system, partly because of the possibility of using these devices as photodetectors. Although the InGaAs-InP system is an important one in optoelectronics, it has been much less studied than the GaAs-AlGaAs system, especially for the perpendicular transport in its heterostructures. To our knowledge, this is the first study of the perpendicular transport in a SL of this system. One reason for the relative lack of work in the InGaAs-InP system is that the growth procedure for this system is not as well established as for the GaAs-AlGaAs system [1]. We observed several series of quasiperiodic Negative Differential Resistances (NDR's) at large applied electric field. Each NDR corresponds to a specific SL period in the device. The observation of a large number of similar and quasi-periodic NDR's demonstrates the high quality of the SL structure. In addition, the large number of NDR's and their regularity open the possibility of using these devices in multiple logic circuits, since one can obtain many equally spaced, stable output voltages for a single current value. Similar effects have been sought in parabolic-well structures and resonant tunneling transistors [3]. We have also studied the temperature and magnetic field dependence of the perpendicular transport in these InGaAs-InP SL's.

This study shows several interesting features. One of these is the formation of a high-field domain in the SL structure at large bias voltage, and its depen-

dence on the temperature and magnetic field applied. The conduction in the high-field domain region is by sequential tunneling from the first subband of one quantum well to a higher subband of the next well. The regular expansion of the high-field domain by one SL period at a time gives rise to the series of NDR's which are quasiperiodic in the applied bias. The period is observed to vary with temperature for the NDR series involving tunneling between the first subband and the second, but is invariant for the tunneling between the first and the third subband. This is due to the variation of the width of the first subband with temperature [4]. When a strong magnetic field is applied perpendicularly to the direction of the tunneling current, the NDR series disappear due to the strong effect of the Lorentz force on the tunneling probability. Another interesting result is the possible observation of miniband conduction in a small fraction of the carriers at low bias. This is relevant to the question of what are the limits on the superlattice periods for observation of miniband conduction, which is being actively pursued as part of the general study of SL transport [5]. Some preliminary results of this work have been reported previously [4].

III.1 Experiment

A schematic diagram of the devices used is shown in Fig. 1. All three samples have barrier width of 80Å . The well widths L_w are 180Å , 300Å and 150Å in samples A, B, and C respectively. Each superlattice consists of 50 periods of nominally undoped InGaAs wells, and unintentionally doped InP barriers. From measurements on a similarly-grown epitaxial layer, the InP layers are estimated to have a donor concentration of $\sim 10^{16}cm^{13}$. To make the device, an AuGeNiCr dot

of 100μm diameter was deposited on the cleaned sample. This forms the top contact of the device. The sample was then mesa-etched down to the second doped contact layer, with the etch depth being monitored with a Dektak machine. For these devices, it was found that etching with the BPK mesa etch, which is a (1:1:1) solution of $HBr:H_3PO_4:K_2Cr_2O_7$, gave good characteristics. The problem with surface leakage conduction present in InGaAs-InP Double-Barrier structures etched with BPK solution [6] did not appear here. This is probably due to the fact that the distance between the two contact layers is fifty times greater in the SL structures than in the double-barrier structures. Therefore, the conductance by surface leakage between the two contact layers should be decreased by a factor of at least fifty in the SL structure.

After the mesa etch, the sample was rinsed in dilute HCl to remove the oxide layer left by the etchant. A second layer of AuGeNiCr was then deposited to form the bottom contact. This layer covered all the sample except for a circle of 200μm diameter which is concentric with the top contact layer. The geometry of the contacts ensures that the applied electric field is perpendicular to the plane of the layers and uniform across the whole mesa. The current vs voltage (I-V) measurements were made using two pairs of leads, one at each contact, to eliminate the leads' resistance from the results.

III.2. Formation of a High-field Domain

When an electric field is applied perpendicularly to the plane of the layers, the I-V characteristics of the three InGaAs-InP superlattices studied have several qualitative features in common. These features are illustrated in Fig. 2. At very

low bias, the conduction is ohmic and symmetrical for the two bias directions. Above a certain critical voltage, which differs for each sample, a series of Negative Differential Resistances (NDR's) is observed. In the following, we shall refer to the I-V characteristics of these two bias ranges as the low-field results and the high-field results. This division is not arbitrary. Experimentally, it was observed that the I-V curves in the two bias ranges depend very differently on temperature, magnetic field, and the sample used.

In the limit of a *small* applied bias, in an ideal SL, the perpendicular conduction is via the superlattice minibands, and is metallic-like. In a real SL, however, the carriers may be localized by phonon or impurity scattering, or by random potential fluctuations, such as caused by monolayer fluctuations at the interface, which can give rise to an Anderson-type localization. Quantitatively, miniband conduction is destroyed when the broadening of the energy levels, w_b, by scattering and by potential fluctuations is of the order of the width of the miniband, w_m, or larger. If miniband conduction is not possible, then the electrons are localized, and conduction occurs by sequential tunneling from one quantum well to the next.

For the case of miniband conduction, at low bias the conduction is metallic and therefore the I-V curve is ohmic. However, as the applied bias voltage V_{bias} is increased, the carriers are localized by the electric field to within a distance

$$L_s = w_m/(eV_{bias}/P) \qquad (1)$$

where P is the number of SL periods, and L_p is the length of each period. L_s is usually called the Stark length. When $L_s \leq L_p$, i.e., when the potential energy drop across each SL period, eV_{bias}/P, is larger than the w_m width of the miniband, the

carriers are field-localized within each SL period [8]. Conduction through the SL then occurs via tunneling. Consequently, the high-mobility miniband conduction ceases for $eV_{bias} \gtrsim Nw_m$, and a drop in the current is expected.

On the other hand, if the electrons are localized even at low bias by scattering or by potential fluctuations, low-field conduction is by sequential tunneling. For $V_{bias} \sim 0$ the conduction would be ohmic ($I \propto V$ to lowest order of V). However, as the bias voltage is increased, when $eV_{bias} \gtrsim Pw_b$, it is no longer possible for electrons to tunnel from one quantum well to the next while conserving both energy and parallel momentum. Thus, for sequential tunneling, the low-field conduction ceases for $eV_{bias} \gtrsim Pw_b$ with $w_b > w_m$.

Experimentally, it is not easy to distinguish between miniband conduction and sequential tunneling from the I-V characteristics at low bias voltage. Both conduction mechanisms are expected to give rise to ohmic behavior at low bias, followed by a decrease in current (i.e., an NDR structure) at some critical bias voltage V_c. Therefore, either of these conduction mechanisms can explain qualitatively the observed low-field behavior of the three samples studied (Fig. 2). Quantitatively, we note that the value of the bias voltage V_1 at which the first NDR occurs is 30 mV $\pm$ 10, 95 mV $\pm$ 5, and 50 mV $\pm$ 5 for samples A, B, and C respectively. The value given is the average for the two bias directions. If miniband conduction were the dominant conduction mechanism, then the first NDR should occur at $V_{bias} = Pw_m/e$, as discussed above. Using simple Kronig-Penney type calculations to calculate the miniband width w_m, the value of (Pw_m/e) is 10 mV, 5 mV, and 10 mV for samples A,B, and C. This is lower than the observed

V_1, and would appear to indicate that the low-field conduction in these samples occur via sequential tunneling, so that V_1 is equal to Pw_b/e, where w_b is the scattering broadened width, and $w_b > w_m$. From the experimental values of V_1, this would give $w_b = 0.6$ meV 1.9 meV, and 1 meV for samples A, B, and C respectively. However, further study of the temperature dependence of the I-V characteristics suggests that, although sequential tunneling is the dominant conduction mechanism, at low temperatures and low bias voltages, there may be some miniband conduction mixed in. This will be discussed in section V.

At higher bias voltages, the I-V curves are dominated by the effect of sequential tunneling between the first subband of the Mth quantum well and a higher subband of the neighboring $(M+1)^{th}$ quantum well, when these subbands are brought to the same energy by the applied bias potential. In the first theoretical calculations of this effect, Kazarinov and Suris [9] assumed that the electric field was uniform throughout the structures. They predicted that the conductance would show large peaks at bias voltages V_n such that

$$eV_n \simeq P(E_n - E_1) \tag{2}$$

where E_n is the energy of the nth subband level. The recent results of Capasso et al. [10], who measured the photoconductivity of an *undoped* $(n^- \leq \times 10^{14} cm^{-3})$ SL as a function of the bias voltage, are in good agreement with the predictions of Kazarinov and Suris [9]. However, in our work, instead of observing a single NDR for each resonance of the 1st to the nth subband, a whole series of NDR's were observed which were quasiperiodic in the bias voltage. This is similar to the early measurements of Esaki and Chang [8], and to the recent works of Choi et al.

[11] and Levine et al. [1] on *doped* (n $\simeq 1\times10^{18}$cm^{-3} in the well) SL's. The observed multiplicity of the NDR's in these SL's is caused by the non-uniformity of the electric field. At low bias, the electric field in a conducting SL is slightly different for each period. This simply may be due to unavoidable inhomogeneity in the SL, as suggested by Esaki and Chang [8]. However, even in an ideal SL, the space charge effect [12] present at any finite current will cause each SL period to experience a different field, with the period nearest to the collector electrode, the P_{th} period, experiencing the greatest field. As the total applied bias voltage is increased from zero, this period will be the first to break off from the alignment of the first subbands [11]. Assuming that there is a gap between the 1st and the 2nd subband of this period is aligned with the 1st subband of the neighboring period. Because most of the potential is now across the Pth period, the potential across the other periods (referred to as the low-field domain from here on) is reduced, resulting in a decrease in the current, and hence the first NDR. Further increase in the bias voltage will give rise first to an increase in the current, because of the increased voltage drop across the low-field domain, but will eventually cause the $(P-1)^{th}$ period to break off from the 1-to-1 subband alignment, and a second NDR is observed. This process repeats at a bias interval of

$$e\Delta V_{1-2} - (E_2 - w_2 - w_1) \qquad (3)$$

where the w_n's are the widths of the nth subbands.

In this simple model, the non-uniform electric field in the SL structure gives rise to a high-field domain. As the bias voltage is increased, the high-field domain expands discontinuously from the positive electrode by one SL period for every ΔV_{1-2} increase in V_{bias}. Each expansion is accompanied by a sharp drop in the

current, and hence a large NDR. There should be (P-1) NDR's for a SL structure with P periods.

The experimental data obtained in our work agree qualitatively with the predictions of the simple model outlined above. The quasiperiodic NDR's of samples A, B, and C occur at bias intervals of 38 mV, 20 mV and 39 mV respectively. These are in rough agreement with the values of ΔV_{1-2} calculated from Eq. (3), which are 44 mV, 23 mV, and 53 mV. The energy levels E_1 and E_2 were calculated from the Kronig-Penney model using a conduction band offset of 220 meV, InGaAs effective mass of $0.045m_o$ for the 1st subbands of all three samples and for the 2nd subband of sample B (for which both E_1 and E_2 are small). For the 2nd subbands of samples A and C, the effect of non-parabolicity was estimated using Kane's model [13] with parameters $E_g = 789$ meV, spin-orbit coupling $\Delta = 360$ meV, and band-edge effective mass of $0.041m_o$. The width of the 1st subband, w_1 is taken to be eV_1/P, where V_1 is the bias voltage at which the first NDR occurs. The width w_2 is not known. For samples A and C, since (E_2-E_1) is large than the LO phonon for InGaAs, it is expected that the largest contribution to w_2 is the relaxation of carriers in the 2nd subband to the ground subband via LO phonon emission. Typical relaxation times would give a subband width of $\lesssim 10$ meV. The value of 10 meV was used for w_2 for samples A and C. For sample B, (E_1-E_2) is smaller than the LO phonon energy, and we have taken the miniband width of 0.2 meV as a lower limit on w_2.

None of the three samples used exhibit as many as (P-1) NDR's for the tunneling between a particular pair of subbands. Sample A comes closest with 47

and 44 for the positive and negative bias polarity, as opposed to the 49 expected. One reason is that some NDR's combine into one, so that a doubling of the voltage interval between NDR's is observed. This may be due to inhomogeneity in a particular period in the SL, so that for this period the orderly formation of the high-field domain due to the space-charge effect does not occur. We also note that the amplitude of the NDR's decreases greatly as the current rises exponentially at the high voltage end of the NDR series. This may cause some NDR's to be unobservable. The reason for this, and more generally for the exponential rise in current, is not understood at present but is probably due to the interplay between the space-charge effect and the tunneling current. The amount of excess charge in each quantum well is proportional to the current [12]. On the other hand, the electric field caused by the space charge modifies the transmission probability of each barrier and hence the magnitude of the tunneling current. In addition, the space charge within the well at the boundary between the low-field and high-field domain has to be consistent with the difference of the electric fields of these two regions. As V_{bias} is increased, the number of SL periods in the low-field domain is decreased. The space-charge on the low-field domain side is distributed over fewer SL periods. Therefore, the transition between the low field and high field becomes more abrupt, and a larger space charge is required at the boundary, which implies a larger current.

Another experimental feature which shows the need for a more detailed theoretical model is the repeatable hysteresis of the I-V curve, as illustrated in Fig. 3 for sample A. Here we have shown the full I-V curve for $V_{bias} \leq 6V$. Within this range,

there are two series of NDR's [4]. The first corresonds to tunneling between subbands 1 to 2, while the second is for tunneling between 1 to 3. For **both** series, the first few NDR's in the series exhibit no hysteresis. However, as the high-field domain expands, the hysteresis between the curves of the up sweep and down sweep increases rapidly. We can rule out external series resistance as the cause, since if this were the case, the hysteresis would increase monotonically with current, whereas it is observed to vanish at the start of the second series of NDR's. For the same reason, it is improbable that the hysteresis is due to some trapping mechanism. The most probable explanation is the role of the space-charge effect. The hysteresis is caused by the space charge being different depending on whether the transition point is approached from the high current side (up curve) or low current side (down curve). Furthermore, if a larger space charge is required at the boundary between the two field domains when the number of periods in the low field domain is decreased, as discussed above, then this would explain the increase of the hysteresis for the latter NDR's in each series as well as its disappearance at the start of each series.

IV.4 Temperature and Magnetic Field Dependence of the High-field Results

a. Temperature Dependence

Figs. 4(a) and 4(b) show the I-V curves of sample A at 4.2K and at 77K respectively. In the low field region, the Ohmic conductance increases by a factor of 2.5 as the temperature is decreased from 77K to 4.2K. At higher bias the first series of NDR's, which corresponds to the tunneling from the 1st to the 2nd

subband, exhibits several differences between the two temperatures. Although the average current is the same, showing that thermionic emission is still negligible at 77K, the amplitude of the current variation at each NDR is greatly increased by lowering the temperature to 4.2K. Fig. 4(c) shows this on enlarged scales. We obsesrve empirically that the increase in the current variation is due both to an increase in the conductance (by a factor of 3), and to an increase in ΔV_{1-2} from 28 meV at 77K to 38 meV at 4.2K. At even higher bias, the second series of NDR's, which corresponds to the tunneling from the 1st to the 3rd subband, shows no strong variation with temperature. The period in the bias voltage for the second series is 59 meV at both temperatures, in fair agreement with the estimated theoretical value of 54 meV, which is the energy gap between the 2nd and 3rd subband (Eq. 3).

As discussed in section III, the positive conductance in the voltage range of the NDR series is expected to be controlled by the conductance of the low-field domain. For the first series of NDR's, the low-field domain conductance is the same as the conductance of the whole SL at very low bias, i.e., in the ohmic conduction region. Therefore, we can understand the three-fold increase of the conductance in the first NDR series as being a reflection of the similar increase in the ohmic conductance. In contrast, for the second NDR series the conduction in the low-field domain is by sequential tunneling between the 1st and the 2nd subband. This tunneling conduction should be nearly temperature-independent, so that the conductance of the whole SL in this bias voltage range is also temperature-independent.

Secondly, the difference in the temperature dependence of the bias voltage period for the two series of NDR's may be explained by the different temperature dependence of the subband widths involved. For the ground subband, it is expected that the subband width w_1 decreases with temperature because of reduced phonon scattering. The decrease in w_1 would result in an increase of ΔV_{1-2} (Eq. 3). In contrast, the widths of the higher subbands are dominated by the effect of the lifetime due to the relaxation to the ground subband via LO phonon emission, and by the effects of inhomogeneities such as monolayer fluctuations. Both these effects are independent of temperature, and they mask the temperature dependence of the phonon scattering contribution to the total subband width. Since the widths of the 2nd and 3_{rd} subbands do not vary with temperature, the energy gap between these two subbands which determines the period of the bias voltage of the second NDR series are also independent of temperature.

b. The Effect of a Parallel Magnetic Field

With the magnetic field in the direction parallel to the layers of the superlattice (i.e., perpendicular to the current direction) the I-V curve exhibits many changes. The main features of the magnetic-field dependence can be explained by two physical effects. Firstly, the change in the momentum due to the Lorentz force leads to the disappearance of the NDR's with increasing magnetic field. Secondly, the localization of carriers by their cyclotron orbits leads to an exponential decrease of the conductance at high magnetic field. These effects can be seen in Figs. 5(a) to 5(i), which show the I-V curves for sample A in the voltage range of the first NDR series, for magnetic field B up to 8T.

The effect of the Lorentz force can be understood as follows. Taking the z-direction to be perpendicular to the plane of SL layers, so that the tunneling current is I_z, and let the B-field be in the y-direction. For an electron traveling in the z-direction with velocity v_z, after time t the Lorentz force changes the electron's momentum in the x-direction $\hbar k_x$ by

$$\Delta(\hbar k_x) = (ev_z B_y)t = eL_z B_y \tag{4}$$

where $L_z = v_z t$ is the distance traveled in the z-direction.

For electrons which have tunneled from one well to another, if they initially have wavevector k_x, then after tunneling into the neighboring well their wavevector is

$$k'_x = k_x + \Delta k_x \tag{5}$$

where

$$\Delta k_x = eL_b B_y/\hbar \tag{6}$$

and L_b is the barrier width.

Thus, in magnetic field B_y, the condition for sequential tunneling for an electron with energy E and parallel momentum of $\hbar k_x$ and $\hbar k_y$ is that there is an available state to tunnel into with energy E and parallel momentum $\hbar k'_x$ and $\hbar k_y$, where $\hbar k'_x$ is given by Eqs. (5) and (6). This can be depicted graphically by shifting the E vs k_x dispersion curve of the initial quantum well (labeled initial states) from which the electron tunnels by an amount Δk_x, given by Eq. (6), with respect to the dispersion curve of the neighboring well (labeled final states) to which the electron tunnels. The states for which tunneling is possible are given by the intersection of these two dispersion curves. This is shown in Figs. 6(a) and

(b). The curve for the initial states is drawn *only* for $k_x \leq k_F$, where k_F is the Fermi wavevector. This represents the initial states which are occupied. The curves are drawn as thin bands of states to show the uncertainty in k_x due to scattering. The initial states' dispersion curve has higher energy relative to the final states by eV_{bias}/P, the potential drop between neighboring wells. It is now easy to explain the disappearance of the NDR's. At zero and small magnetic fields, NDR's are observed because as the bias voltage between the two wells are increased, the current decreases from a finite value when there is tunneling between the ground subbands, to zero when the initial-state dispersion curve is between the final-state dispersion curves of the ground and first excited subbands (Fig. 6(a)). Thus, the NDR occurs because there is a range of voltage for which there are no states allowed for sequential tunneling. As the magnetic field is increased, for $B \geq B_c$, the shift Δk_x is large enough that at any voltage, the initial state dispersion curve intersects with the dispersion curve of either the first or second subband, or both (Fig. 6(b)). Therefore, there are no NDR for $B \geq B_c$. The critical field B_c can be calculated from the condition

$$\hbar^2/2m(\Delta k_c + k_F)^2 = \hbar^2/2m(\Delta k_c - k_F)^2 + \Delta V_{1-2} \tag{7}$$

where $\Delta k_c = eL_bB_c/\hbar$ is the shift in the dispersion curve due to B_c. Assuming a typical electron concentration of $2\times10^{11}\text{cm}^{-2}$, and taking the experimental value of 38 meV for ΔV_{1-2}, B_c is estimated to be 6 Tesla, in agreement with the data of Fig. 6 which show that all NDR structures disappear for $B \geq 6$ Tesla.

The second major change in the I-V curve with magnetic field is the decrease in the conductance. In Fig. 7, the conductance at $V_{bias} = 0.2\text{V}$ is plotted as a

function of the magnetic field. For B≤1 Tesla, the conductance is constant. For higher values of B, the conductance decreases rapidly. For B≥4 Tesla, it appears to be decreasing exponentially with field as exp(-0.93 · B). We note that at 1 Tesla, the cyclotron length is 257Å which is almost exactly equal to the SL period of 260Å . Thus, for magnetic fields larger than 1 Tesla, the cyclotron length, which is one possible localization length for the carriers, becomes smaller than the SL period, and the localization of the carriers by the magnetic fields becomes effective and decreases the tunneling current. In the high B-field limit, calculations [14] show that the tunneling current varies with B roughly as $\exp(-L_o^2/2L_c^2)$, where L_o is the weighted average tunneling length which it taken to be the barrier width L_b, and L_c is the cyclotron length. For $L_b = 80$Å , the calculations would predict that the current decreases as exp(-5.1 · B). The exponential behavior is observed, but the measured exponent is nearly six times smaller than the predicted value. The cause for this discrepancy is not understood at present.

Finally, Fig. 8 shows the increasingly stronger dependence of the tunneling current on the applied voltage, as the magnetic field is increased. This is because the shift Δk_x due to the magnetic field is a significant fraction of the Brillouin boundary of the SL, $k_{Brillouin} = \pi/L_p$. For example, a 8 Tesla, $\Delta k_x = 0.8k_{Brillouin}$. The explanation is as follows. As the bias voltage is increased, the intersection between the initial and final dispersion curves which represents the allowed tunneling states moves towards the zone boundary, and the number of allowed states is increased. This increase in the number of allowed states with bias voltage provides an extra factor in the voltage-dependence of the current. As

the B-field is increased, Δk_x is increased, the intersection of the two dispersion curves moves nearer to the boundary, and the change in the number of allowed states for a given change in the bias voltage becomes correspondingly larger. Thus, the total voltage-dependence of the current increases with magnetic field.

c. The Effect of a Perpendicular Magnetic Field

It is expected that an applied B-field in the direction perpendicular to the lattice layers would have little effect on the tunneling conduction. Figs. 9(a) and (b) show the behavior of the first NDR series in a perpendicular magnetic field up to 8T. In comparison with the effect of the parallel B-field, there is little change in the I-V curve. All the NDR's are still present at the highest B-field. The only change is a slight increase in the average current as the field is raised to 8 Tesla. This increase is similar, although smaller than, the increase observed when the **parallel** magnetic field was increased to 1 Tesla. It is probably due to a slight misalignment of the sample with respect to the field direction, so that there is a small parallel field component present at the highest nominally perpendicular applied field.

III.5 Temperature and Magnetic Field Dependence of the Low-field Results

a. Temperature Dependence

In the low-field region, the transport mechanisms are: phone-assisted tunneling (hopping). thermal emission over the barriers, sequential tunneling, impurity-assisted tunneling, and miniband conduction. The first two conduction

mechanisms decrease rapidly with temperature and are generally negligible below liquid nitrogen temperature. The next two mechanisms are temperature-independent if the temperature dependence of the Fermi level can be neglected, which is the case for 2-D structures with typical electron concentrations. In contrast, with the metallic-type conduction of minibands, the mobility is expected to increase with decreasing temperature, leading to an increase in the conduction.

The temperature dependence of the low-field, Ohmic conduction of samples A, B, and C are shown in Fig. 10. It is clear from Fig. 10 that the behavior of sample C is qualitatively different from the other two, despite the fact that the high-field data for the three samples are quite similar. The low-field conductance of sample C decreases with decreasing temperature from 300K to 110K, and remains constant for temperatures down to 4.2K. The initial decrease in the conductance is due to the decrease of the thermionic emission and hopping contributions. For $T < 110K$, these contributions are negligible, and the conduction is dominated by the sequential tunneling mechanism which is temperature-independent in this range of temperature. In contrast, both samples A and B show a minimum in the conductance at $\sim$ 110K. Below this temperature, the conductance shows a large increase with decreasing temperature. For sample A, there is a three-fold increase of the conductance from 110K to 4.2K. We attribute this remarkable behavior to the presence at low temperature of some miniband conduction mixed in with the sequential tunneling conduction.

Initially, it was not expected that these devices would show any miniband conduction because the 80Å barriers give rise to small miniband widths of less

than 0.2 meV for the lowest miniband. As discussed in section III, this implies that the broadening by inhomogeneity and by scattering has to be less than 0.2 meV for miniband conduction to occur, which does not seem likely. However, at low temperatures where phonon scattering becomes negligible, the main hindrance to miniband conduction is the Anderson-type localization by the potential fluctuations due to inhomogeneity in the sample, such as monolayer fluctuations at the interfaces. This type of localization gives rise to a broadened energy band where the states in the low and high energy tails are localized, and there is a narrow range of energy at the center of the band where the states are extended. For the following discussion the important consequence of this model is that there is a critical energy above which carriers can travel freely through the superlattice, i.e., miniband conduction is possible for carriers with high enough energy. It is thus possible that below 120K, as the phonon scattering decreases and Anderson localization becomes the main hindrance to metallic conduction, an increasing, though small, fraction of the electrons which have energies above this critical energy are showing miniband conduction. These electrons would have a large effect on the total conduction because their mobility is expected to be several orders of magnitude larger than the effective mobility of sequential tunneling. Assuming that the relevant miniband effective mass is similar to that of the bulk, the mobility of the miniband-conduction electrons should be approximately that of the bulk materials, which is $\sim 5000 cm^2V^{-1}s^{-1}$. From the measured conductance, the effective mobility for sample A at 4.2K is $2.3 cm^2V^{-1}s^{-1}$. This low average mobility is typical of sequential tunneling, and shows that the conduction is dominated by sequential tunneling even at low temperature. For example, Choi et al, [11]

measured the mobility at 5K for sequential tunneling to be $0.12 cm^2 V^{-2} s-1$. On the other hand, the much higher mobility of miniband conduction makes it feasible that the increase in the small number of electrons participating in miniband conduction could account for the increase in the total conductance as the temperature is decreased. This effect becomes more pronounced as the mobility of the metallic-like miniband conduction increases with decreasing temperature.

b. The Effect of a Parallel Magnetic Field at Low Temperature

The magnetic-field dependence of the low-field resistance for temperature below 4.2K is shown in Figs. 11(a) and (b). In this low temperature range, the I-V curve in the low-field region is no longer Ohmic, with the conductance increasing with applied bias voltage. The solid curves show the resistance as a function of the parallel magnetic field at 1 mV for different temperatures. At low B-field, the device shows a negative magnetoresistance which becomes more pronounced as the temperature is decreased below 4.2K, both in absolute magnitude (Fig. 11(a)) and as a percentage of the zero-field resistance (Fig. 11(b)). For $B \gtrsim 0.15$ Tesla, the magnetoresistance is positive, and is again larger for the lower temperatures. The set of dotted curves shows the magnetoresistance at 0.3K for bias voltages of 1 mV, 5 mV, 10 mV, and 15 mV. The corresponding values of eV_{bias}/P, which is the energy gained by the carriers in tunneling across each SL period, are 0.2K, 1.2K, 2.3K, and 3.5K. A comparison of the solid and dotted curves in both Figs. 11(a) and (b) show that there is a remarkable similarity between the magnetoresistance curve obtained a 1 mV and sample temperature T_s, and the curve obtained at $T_s = 0.3K$ and V_{bias} such that the energy gained per SL period is

$\sim T_s$. At present, we are not aware of any appropriate theoretical calculations on the magnetoresistance of the tunneling transport in the low B-field range. We are currently working on this problem in order to analyze these data, in particular the large negative magnetoresistance seen, and the correspondence between the solid and dotted curves.

III.6 Conclusion

In this study of InGaAs-InP superlattices, we have observed that, similar to the GaAs-AlGaAs superlattices, the perpendicular transport shows an Ohmic behavi... low field and a series of quasiperiodic NDR structures at high field. The high field behavior is caused by the formation of a high-field domain within the superlattice. This domain formation is probably initiated by the electric field due to the space charge accumulated at finite current. The NDR series which is caused by this domain formation disappears at high parallel magnetic field due to the shift in the momentum by the Lorentz force. These main points in the understanding of the high field results are well supported by the experimental observations. However, more theoretical work is needed to clarify the role of the space charg... fect in the sequential tunneling conduction. In particular, the dependence of the ... erage current and of the hysteresis on the spatial extent of the high-field dom... are not well understood at present. In addition, the temperature dependenc... the low field Ohmic conductance appears to indicate the present of some minil... d conduction mixed in with the dominant sequential tunneling conduction. ... spite the large superlattice periods of these devices. Further theoretical work ... needed to interpret the low field results especially regarding its magnetic

field dependence.

References

* Based on unpublished work by T.H.H. Vuong, D.C. Tsui and W.T. Tsang.

1. B.F. Levine, K.K. Choi, C.G. Bethea, J. Walker and R.J. Malik, Appl. Phys. Lett. **50**, 1092 (1987); K.K. Choi, B.F. Levine, C.G. Bethea, J. Walker, and R.J. Malik, Appl. Phys. Lett. **50**, 1814 (1987).

2. W.T. Tsang, Appl. Phys. Lett. **45**, 1234 (1984).

3. S. Sen, F. Capasso, A.C. Gossard, R.A. Spah, A.L. Hutchinson, and S.N.G. Chu, Appl. Phys. Lett. **51**, 1428 (1987); S. Sen, F. Capasso, A.Y. Cho, D.L. Sivco, IEEE Electron Device Lett. **9**, 533 (1988); F. Capasso, S. Sen, A.Y. Cho, and D.L. Sivco, Appl. Phys. Lett. **53**, 1056 (1988).

4. T.H.H. Vuong, D.C. Tsui and W.T. Tsang, Appl. Phys. Lett. **52**, 981 (1988); ibid, Superlattices and Microstructures, **4**, 207 (1988).

5. B. Deveaud, J. Shah, T.C. Damen, B. Lambert and A. Regreny, Phys. Rev. Lett. **58**, 2582 (1987); J.F. Palmier, C. Minot, J.F. Lievin, F. Alexandre, J.C. Harmand, J. Dangla, C. Dubon-Chevallier and D. Ankri, Appl. Phys. Lett. **49**, 1260 (1986); R.A> Davies, M.J. Kelly and T.M. Kerr, Phys. Rev. Lett. **55**, 1114 (1985).

6. T.H.H. Vuong, D.C. Tsui, W.T. Tsang, Appl. Phys. Lett. **50**, 1004 (1987).

7. L. Esaki and R. Tsu, IBM J. Res. Dev. **4**, 61 (1970).

8. L. Esaki and L.L. Chang, Phys. Rev. Lett. **33**, 495 (1974).

9. R.F. Kazarinov and R.A. Suris, Sov. Phys. Semicond. **5**, 707 (1971); ibid, **6**, 120 (1972).

10. F. Capasso, K. Mohammed and A.Y. Cho, Appl. Phys. Lett. **48**, 478 (1986).

11. K.K. Choi, B.F. Levine, R.J. Malik, J. Walker and C.G. Bethea, Phys. Rev. B**35**, 4172 (1987).

12. V.J. Goldman, D.C. Tsui and J.E. Cunningham, Phys. Rev. Lett. **58**, 1256 (1987); ibid, Phys. Rev. B**35**, 9387 (1987).

13. T. Hiroshima and R. Lang, Appl. Phys. Lett. **49**, 456 (1986).

14. B. Movaghar, Semicond. Sci. Technol. **2**, 207 (1987).

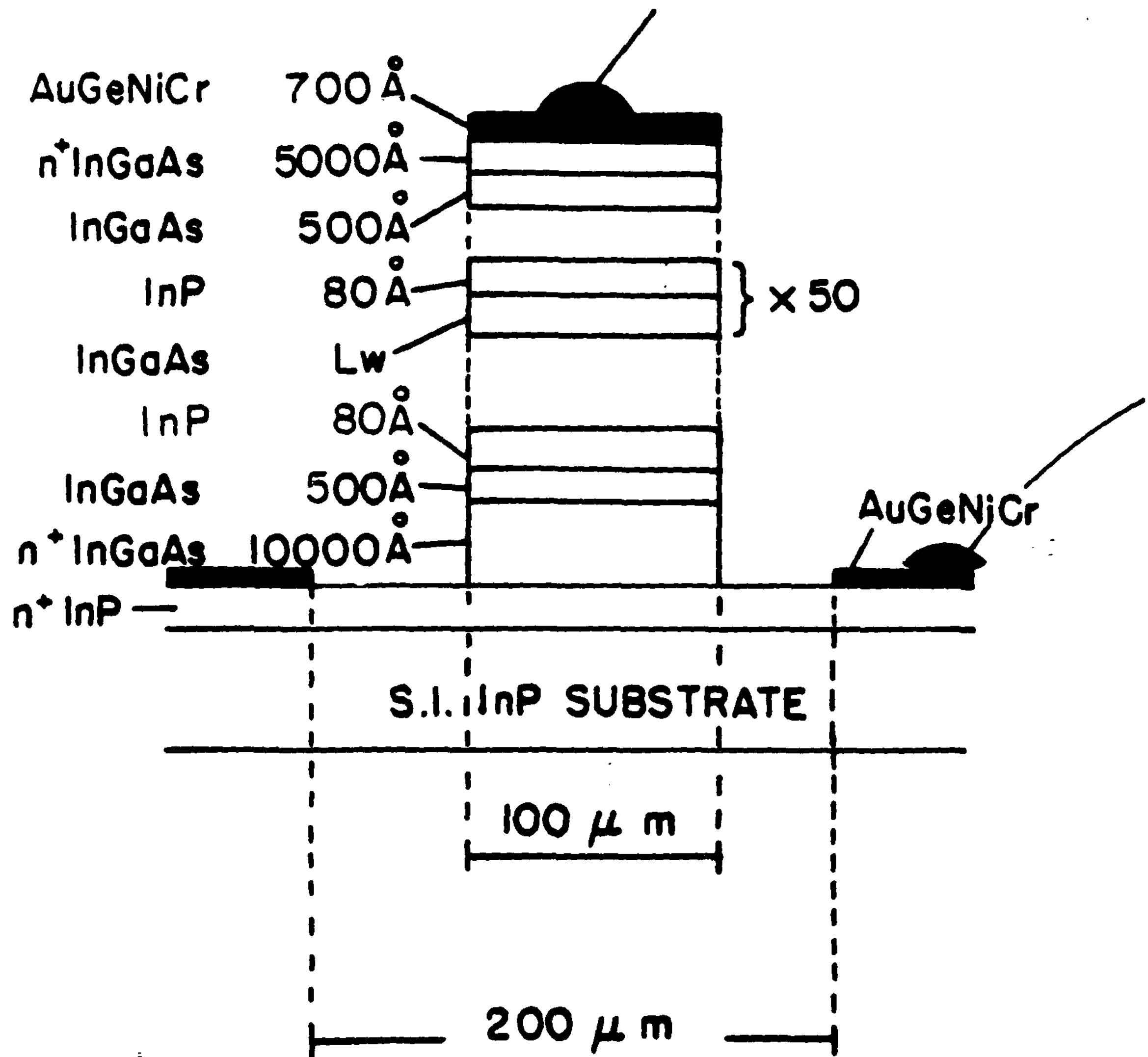

Figure 1: The schematic diagram of the superlattice devices used in this study of the transport in the direction perpendicular to the plane of the superlattice layers. The well width L_w is 180Å, 300Å, and 150Å for samples A, B, and C respectively.

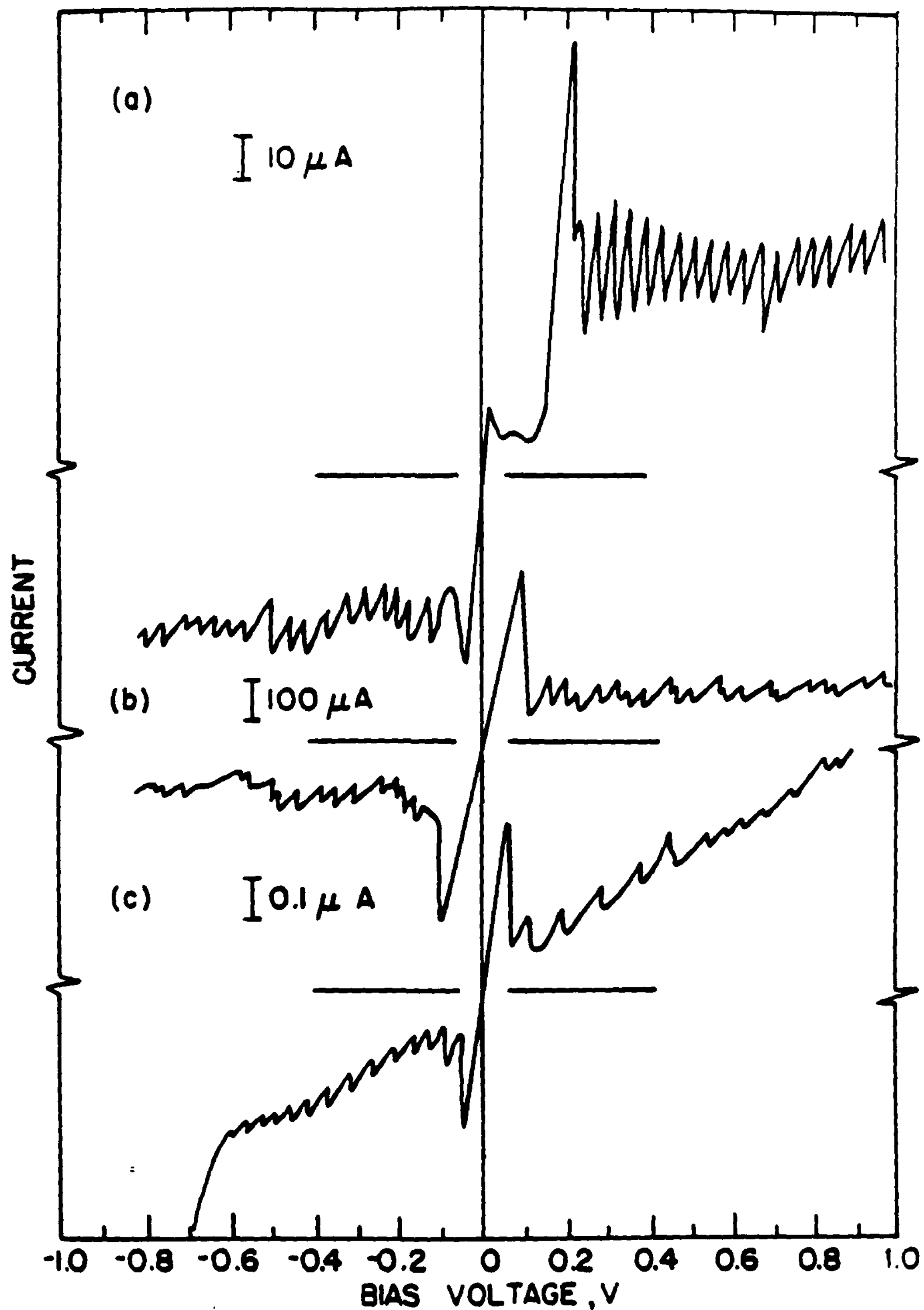

Figure 2: Curves (a), (b), and (c) show the I-V characteristics at 4.2K for samples A, B, and C respectively. All three samples show an ohmic conduction region at low bias voltage, and a series of quasiperiodic NDR's at higher bias.

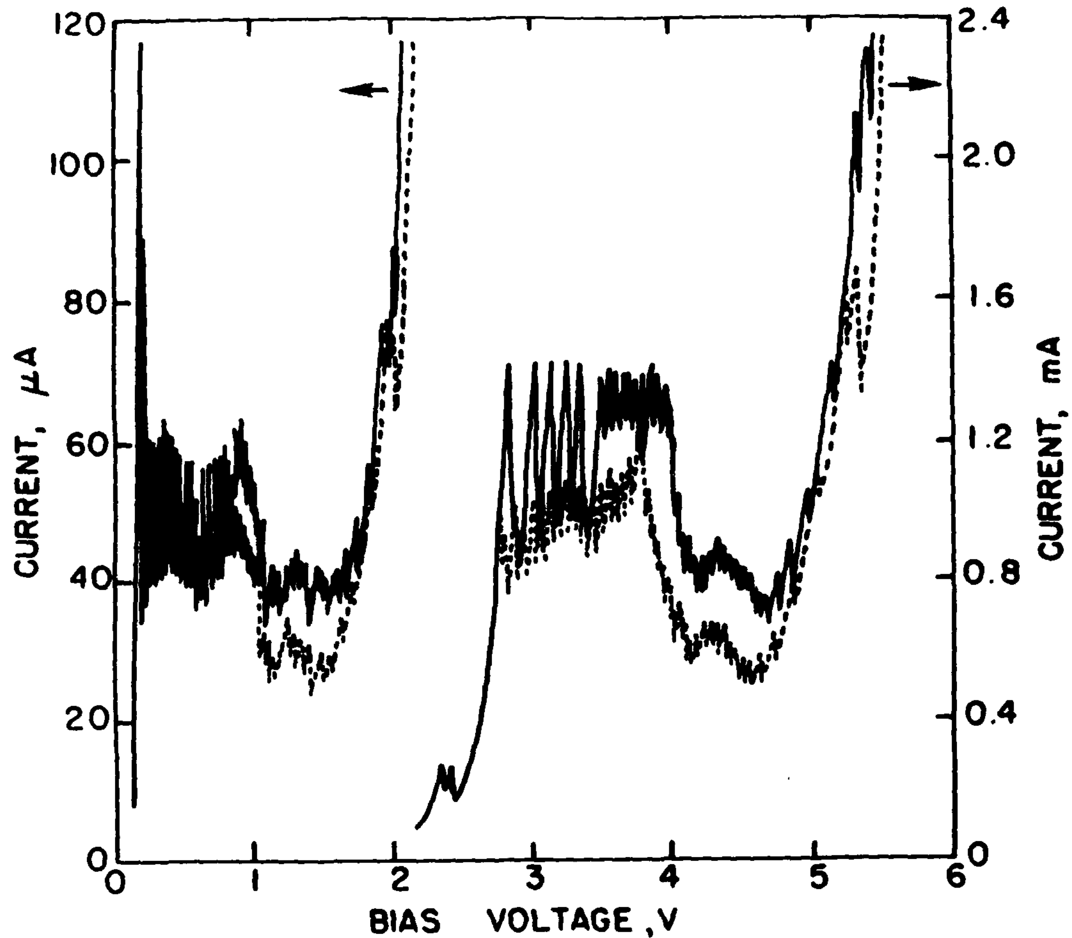

Figure 3: The full I-V characteristics of sample A at 4.2K, showing two series of NDR's. The first series corresponds to sequential tunneling from the ground subband of one well to the 2nd subband of the neighboring well. The second series of NDR's corresponds to tunneling from the ground subband to the 3rd subband. The solid curve is the trace obtained when the bias voltage is swept up. The dotted curve is for the down sweep. We note that the hysteresis between the two curves vanish at the start of each of the two series of NDR's.

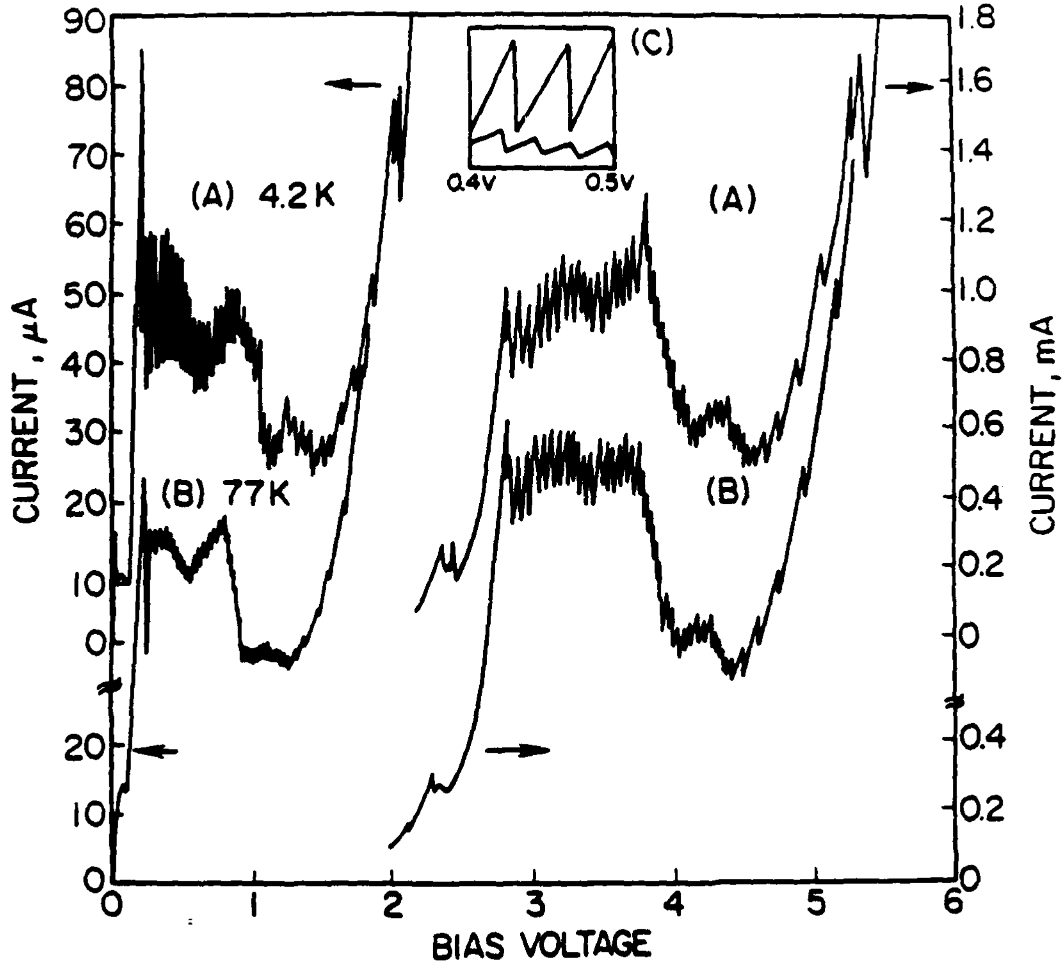

Figure 4: The I-V characteristics of sample A at (A) 4.2K and (B) 77K. These show large differences for the first series of NDR's, but very little for the second series. The inset (C) shows a portion of the first NDR series in greater details, with the upper curve being the 4.2K results, and the lower curve the 77K results.

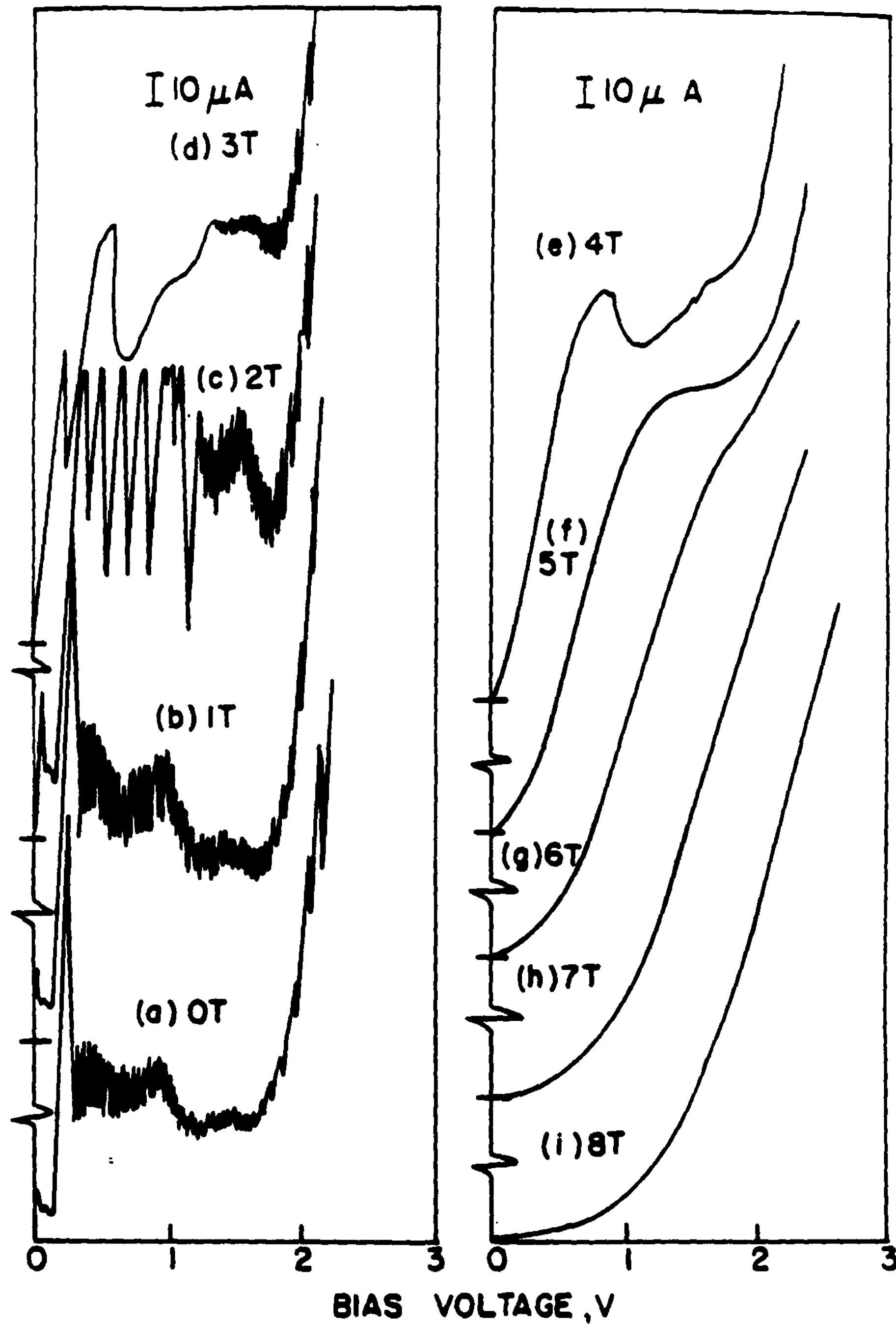

Figure 5: The magnetic field dependence of the first series of NDR's for sample A at 4.2K. Curves (a) to (i) show the results from 0 to 8 Tesla, with 1 Tesla interval between each curve.

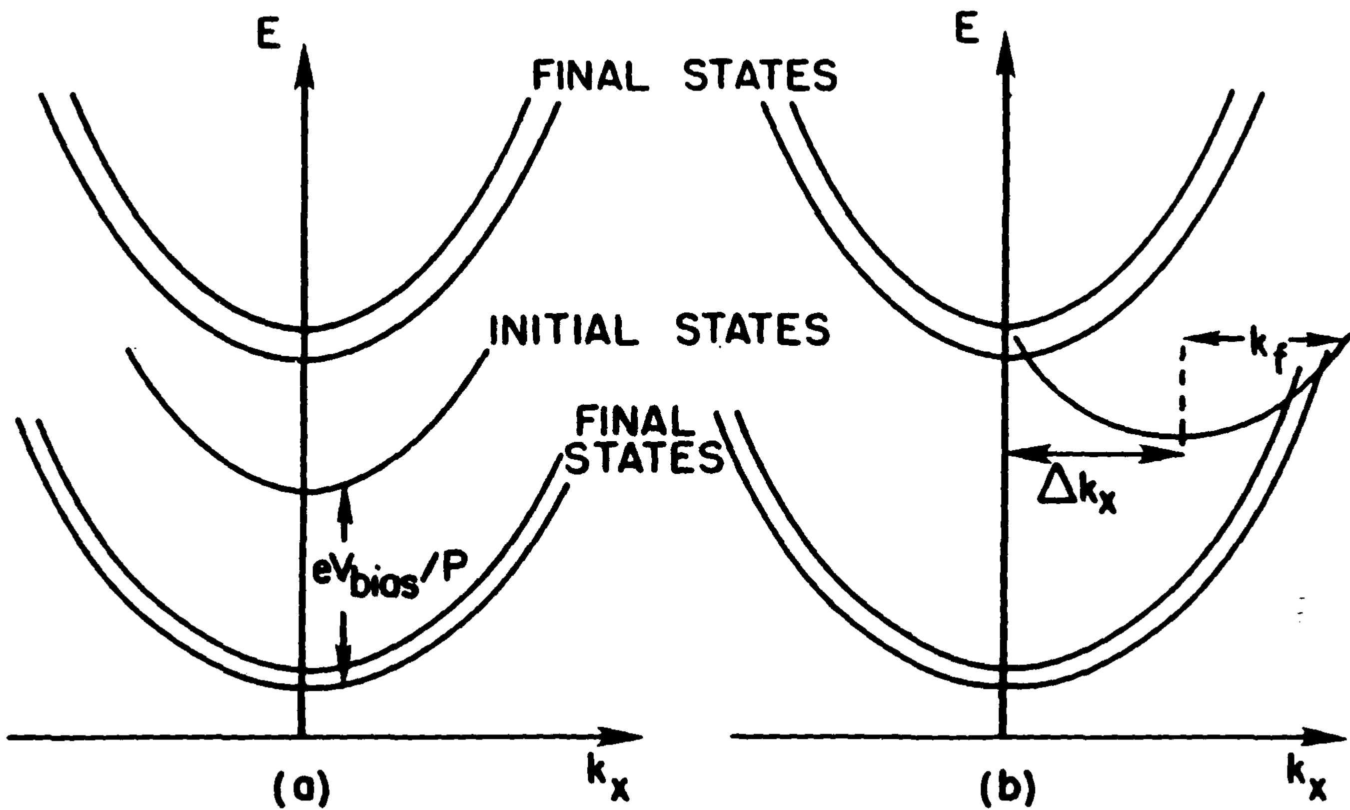

Figure 6: Schematic diagrams of the E vs k_x dispersion curves are shown. For the initial states from which the carriers tunnel, only the states with momentum less than or equal to the Fermi wavevector are shown. For the final states, the dispersion curves of both the first and second subbands are shown. Figure 6(a) depicts the situation when there is no magnetic field applied, or only a small field. At the bias voltage shown, there are no intersection between the initial and final states curves. Thus there are no states available for resonant tunneling, and an NDR feature should be observed at this bias. In Fig. 6(b), there is a large parallel magnetic field which shifts the initial states' dispersion curve by Δk_x. The dispersion curves now intersect, and no NDR is observed.

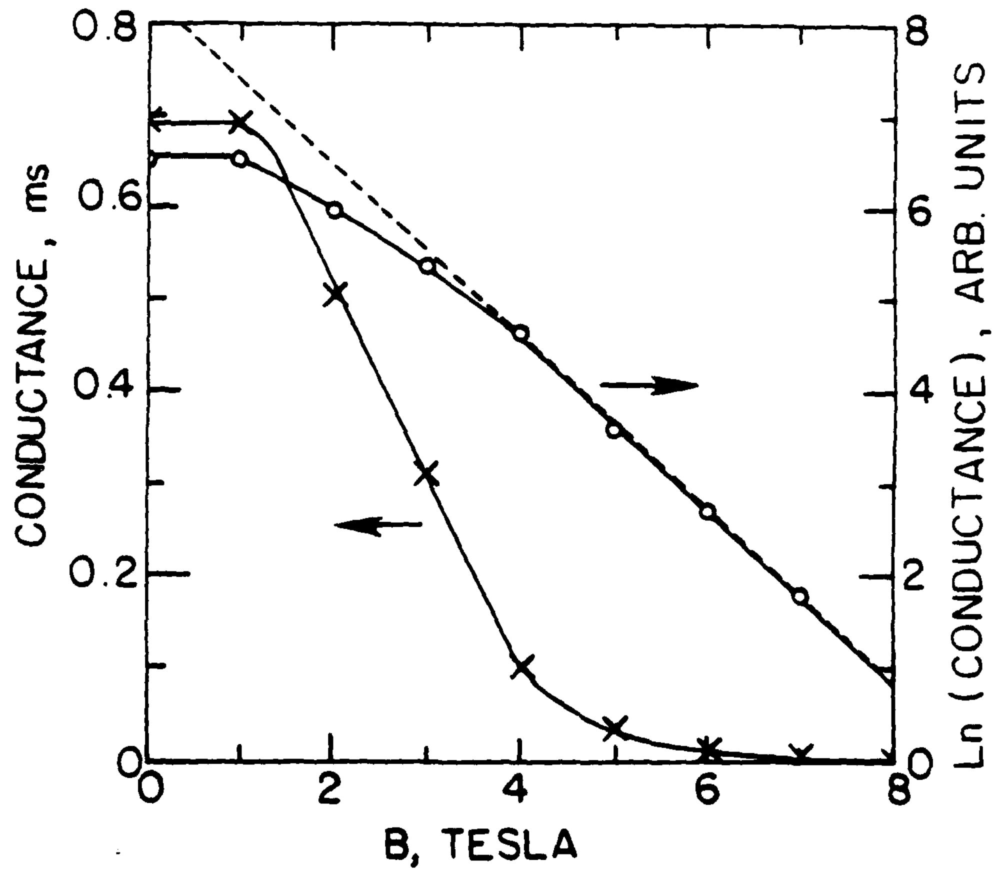

Figure 7: The conductance at 0.2 V and 4.2K, and its logarithm are plotted as a function of the magnetic-field B. For B ≥ 4 Tesla, the conductance varies as exp(−0.93B).

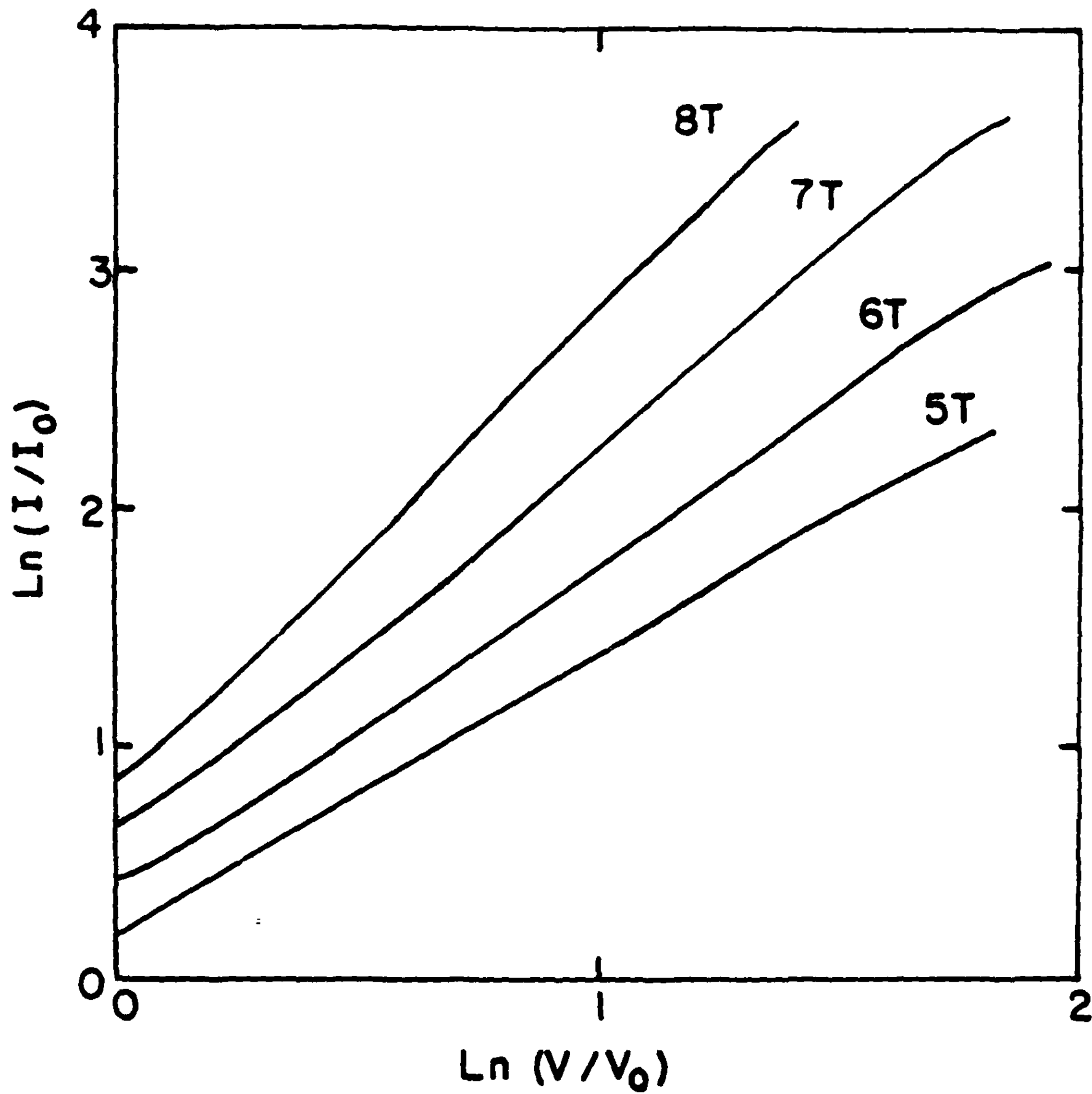

Figure 8: Ln (I/I_0) vs Ln (V/V_0) is plotted for several magnetic field, showing the increasingly non-ohmic behavior at high B-field. I_0 and V_0 are arbitrary, chosen to make the graphics clear.

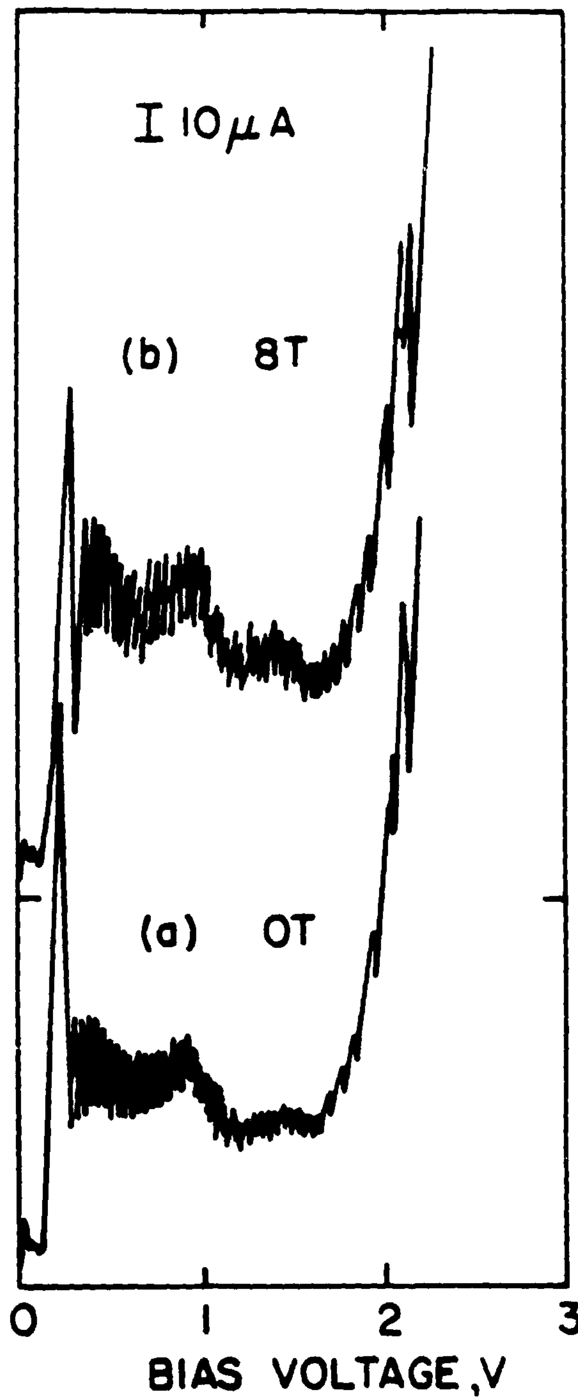

Figure 9: Curves (a) and (b) are the I-V characteristics of sample A at 4.2 K, at 0 and 8 Tesla respectively, with the magnetic field direction perpendicular to the plane of the SL layers.

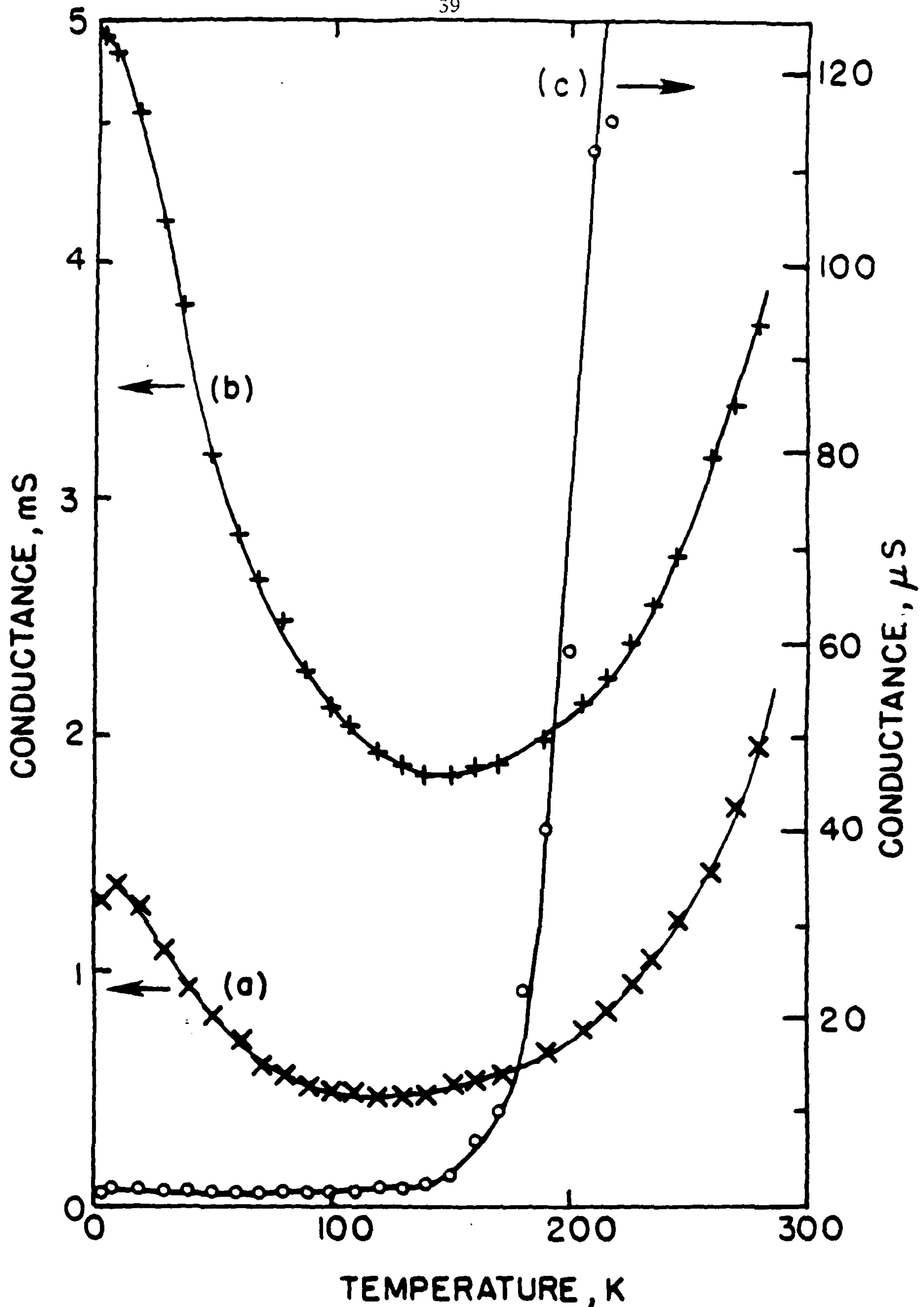

Figure 10 The temperature dependence of the low field conductance of (a) sample A, (b) sample B, and (c) sample C. The increase in the conductance of samples A and B at low temperatures may indicate the increasing effect of miniband conduction.

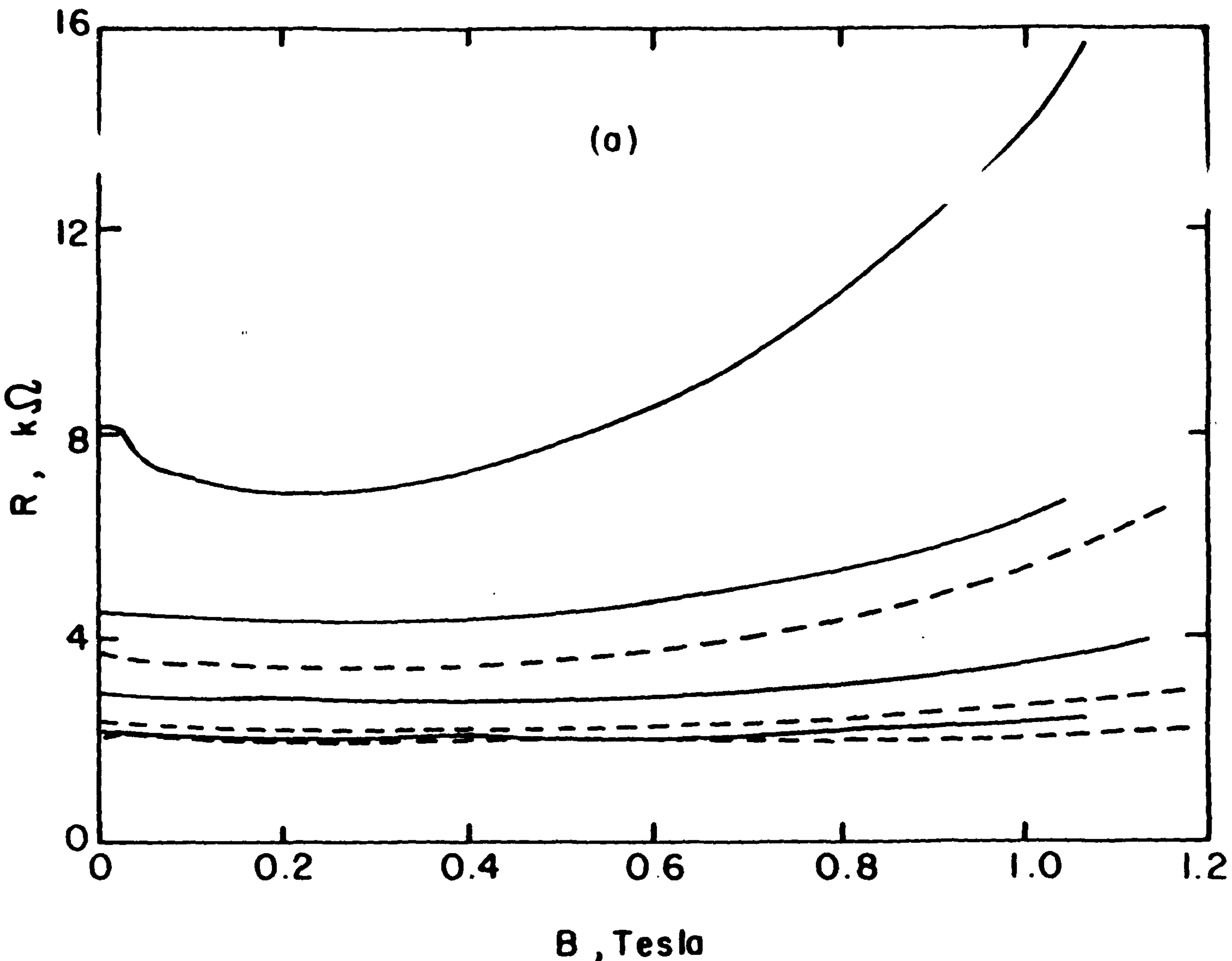

Figure 11: (a) The resistance vs B curves of sample A. The solid curves show the resistance at V_{bias} = 1 mV, obtained at 0.3K, 1.5K, 2.2K, and 3K with the curve for the lowest temperature having the highest resistance values. The dotted curves show the resistance vs B at 0.3K for V_{bias} = 5mV, 10mV, and 15mV, with the curve for the lowest bias having the highest resistance values.

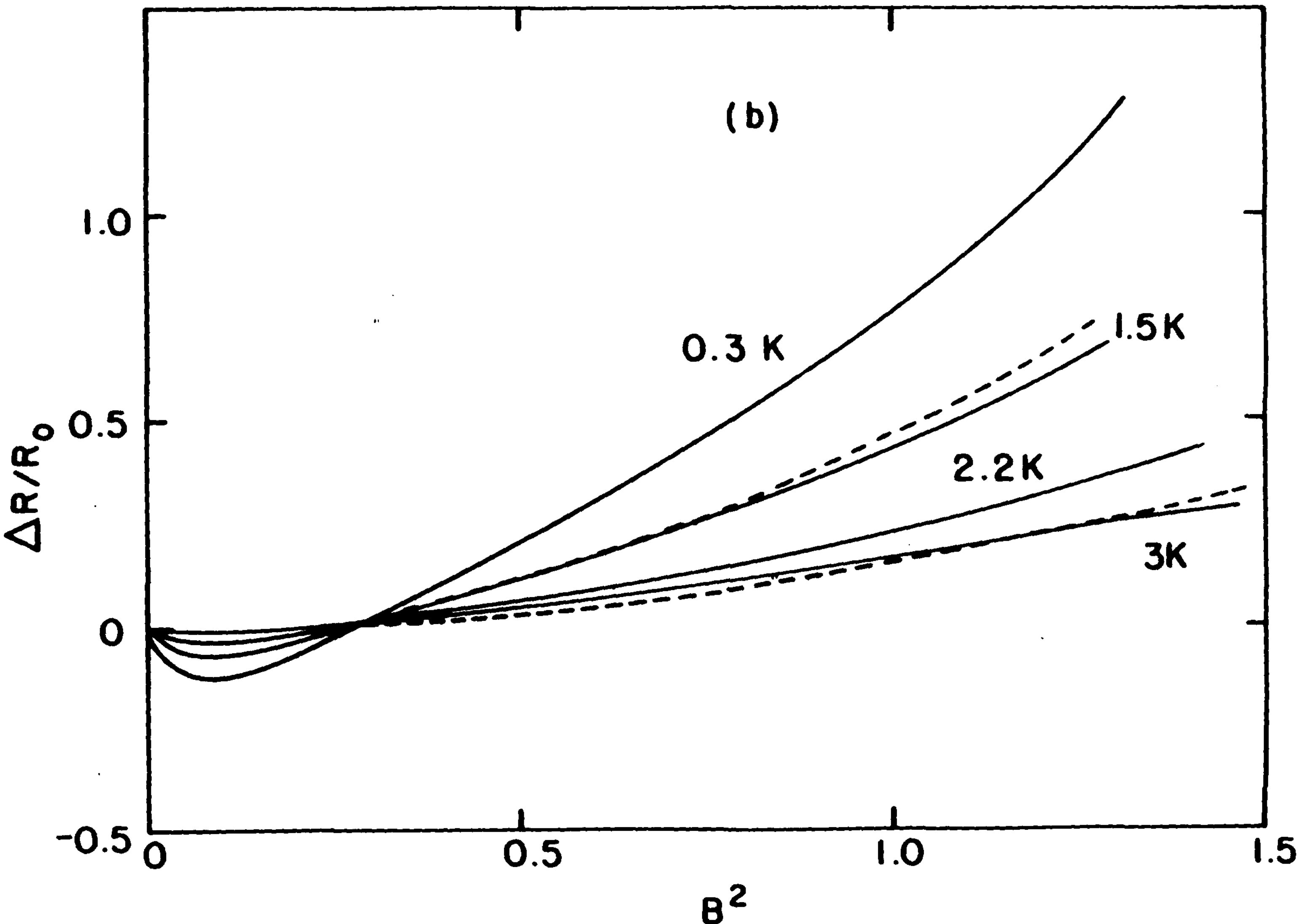

Figure 11: (b) The normalized magnetoresistance vs B^2 curves of sample A. The solid curves were obtained at V_{bias} = 1 mV, and at 0.3K, 1.5K, and 3K, with the curve at lowest temperature showing the largest normalized magnetoresistance values. The dotted curves were obtained at 0.3K, with V_{bias} = 5 mV and 10 mV, with the curve at lower bias showing the larger normalized magnetoresistance values.